Prostate Cancer and Prostatic Diseases (2017) 20, 430–435

www.nature.com/pcan

ORIGINAL ARTICLE

Molecular alterations in prostate cancer and association with MRI features

D Lee[1,7], J Fontugne[2,3,7], N Gumpeni[4], K Park[2], TY MacDonald[2,3,5], BD Robinson[1,2,3,5], A Sboner[1,3,5,6], MA Rubin[1,2,3,5], JM Mosquera[1,2,3,5,8] and CE Barbieri[1,2,5,8]

BACKGROUND: Multiparametric magnetic resonance imaging (mpMRI) has been increasingly used for prostate cancer (PCa). Recent studies identified distinct molecular subclasses of PCa with recurrent genomic alterations. However, the associations between molecular alterations in PCa and characteristics on mpMRI are unknown. Therefore, the objective of this study was to investigate recurrent molecular alterations in PCa and their associations with mpMRI features.

METHODS: Sixty-two PCa nodules >0.5 cm had a preoperative mpMRI. Nodules were evaluated for *ERG* rearrangement, *PTEN* deletion, *SPINK1* overexpression, *SPOP* mutation and *CHD1* deletion. Each PCa focus was matched to the corresponding location on mpMRI. Lesions were scored by single observer according to the PI-RADSv2 scale.

RESULTS: Of the 62 nodules, 22 (35.5%) were *ERG* positive, 6 (9.7%) had SPINK1 overexpression, 6 (9.7%) had *SPOP* mutations, 4 (6.5%) had *CHD1* deletions and 1 (1.6%) had *PTEN* deletion. All of the nodules with *CHD1* deletions were not visible on mpMRI ($P=0.037$). All of the nodules with SPINK1 overexpression were visible on mpMRI, although the association was not statistically significant ($P=0.06$). There were no significant associations between any molecular alteration with the severity of the PI-RADS scores (all $P>0.05$).

CONCLUSIONS: This investigation represents the first description of an association between recurrent molecular alterations and the characterization of PCa nodules on mpMRI. This study can be considered hypothesis-generating for future studies to rigorously evaluate the association of specific PCa molecular subclasses with imaging features and potentially define specific subsets of PCa for which the utility of MRI is higher or lower.

Prostate Cancer and Prostatic Diseases (2017) **20,** 430–435; doi:10.1038/pcan.2017.33; published online 1 August 2017

INTRODUCTION

Prostate cancer (PCa) is a common but clinically and molecularly heterogeneous disease. Many of these men will have aggressive disease, with up to 40% experiencing disease progression despite primary treatment.[1] For other men, PCa will not affect their normal lifespan,[2] and they may experience significant morbidity and compromised quality of life after PCa treatment.[3]

The significant public health burden of overtreatment has led to increased interest in prognostic biomarkers. Recent integrative analyses of gene expression, copy number alterations and chromosomal rearrangements have confirmed distinct molecular subclasses[4,5] with mutually exclusive genomic and transcriptomic events within PCa,[6–8] especially between ETS fusion-positive and ETS fusion-negative PCa.[7] The most common alteration in PCa involves gene fusions of androgen-regulated genes and ETS transcription factors, most commonly TMPRSS2-*ERG* fusion,[8] present in 30–50% of cases.[9–13] Consistent with results from population-based cohorts,[14] a recent study of patients on active surveillance found that the presence of *ERG* translocation in the biopsy specimen was the most significant predictor of progression.[15] We first reported somatic mutations in the Speckle-Type POZ Protein (*SPOP*) gene in 6–15% of PCas.[7] *SPOP* mutations define a distinct subclass of PCa: *SPOP* mutations and *ETS* rearrangements are mutually exclusive, *SPOP* mutant prostate tumors generally lack lesions in the PI3K pathway, and they are also independent of mutations in the tumor suppressor gene *TP53*.[7,16] Therefore, molecular subtyping in PCa may help improve risk-prognostication, and also facilitate more personalized and directed therapies.

Recent advances in multiparametric magnetic resonance imaging (mpMRI) have also improved PCa risk stratification. Numerous studies have found that the application of mpMRI can improve the sensitivity and specificity of detecting clinically significant PCa,[17] and MRI-guided targeting may improve prostate biopsy performance.[18] However, little is known about the associations between molecular and genomic alterations and characteristics on mpMRI. The goal of this study was to characterize recurrent molecular alterations in PCa and their associations with features on mpMRI.

MATERIALS AND METHODS

Patient population

Forty-eight radical prostatectomy (RP) specimens from a single institution between 2008 and 2012 were included in the study (Weill Cornell

[1]Department of Urology, Weill Cornell Medicine and New York-Presbyterian, New York, NY, USA; [2]Department of Pathology and Laboratory Medicine, Weill Cornell Medicine and New York-Presbyterian, New York, NY, USA; [3]Caryl and Israel Englander Institute for Precision Medicine, Weill Cornell Medicine and New York-Presbyterian, New York, NY, USA; [4]Department of Radiology, Weill Cornell Medicine and New York-Presbyterian, New York, NY, USA; [5]Sandra and Edward Meyer Cancer Center, Weill Cornell Medicine and New York-Presbyterian, New York, NY, USA and [6]Department of Computational Biomedicine, Weill Cornell Medicine and New York-Presbyterian, New York, NY, USA. Correspondence: Dr. JM Mosquera, Department of Pathology and Laboratory Medicine, Weill Cornell Medicine and New York-Presbyterian, 1300 York Avenue, New York, NY 10065, USA or Dr. CE Barbieri, Department of Urology, Weill Cornell Medicine and New York-Presbyterian, 1300 York Avenue, New York, NY 10065, USA.
E-mail: jmm9018@med.cornell.edu or chb9074@med.cornell.edu
[7]These authors contributed equally to this work.
[8]These authors share senior authorship.
Received 14 March 2017; revised 22 May 2017; accepted 4 June 2017; published online 1 August 2017

Medicine/New York-Presbyterian Institutional Review Board protocol# IRB 1007011157). These cases are part of the well-characterized Early Detection Research Network (EDRN) cohort.[19,20] A total of 98 discrete PCa nodules were identified. Patient characteristics are listed in Table 1. Patients were included in the study if they had a corresponding preoperative mpMRI performed. None of the authors have any relevant disclosure or conflicts of interest to report. Sources of funding are provided in the acknowledgement section.

MRI acquisition and analysis

All MRI examinations were performed on MRI units at field strengths of 1.5 or 3 Tesla and featured the use of a pelvic phased-array coil with four channels with or without an endorectal coil. The dedicated MRI protocol included a T2-weighted sequences in axial, coronal and sagittal planes, diffusion-weighted sequence with b-values of 0 and 1000 s mm^{-2} (single-shot spin-echo EPI sequence; TR = 3500–5600, TE = 70.3/105.6; slice thickness: 3 mm, no interslice gap; field of view: 14 × 14–24 × 24 cm; matrix: 128–128) and a T1-weighted dynamic contrast-enhanced sequence (TR = 3.6–4.9 ms, TE = 1.3–1.7 ms; slice thickness: 5 mm, no interslice gap; field of view: 24 × 24 cm; matrix: 256x128–160, mean temporal resolution: 10 s). ADC maps were generated from diffusion-weighted images on a voxel-wise basis using a monoexponential model. Image acquisition was begun after intravenous injection of 0.1 mmol of gadopentetate dimeglumine per kilogram of body weight (Magnevist; Berlex Laboratories, Montville, NJ, USA) at a rate of 2 ml s^{-1} using an automatic injector (Medrad, Indianola, IA, USA).

Lesion rating system

Prostate lesions detected on MRI were graded according to the Prostate imaging, reporting and data system scoring, version 2 (PIRADSv2),[21] which scores the radiologist's opinion regarding the likelihood of the presence of PCa on a scale from 1 to 5, with 5 carrying a high-diagnostic likelihood of PCa. As the PIRADS grading system changed in 2015, which is after the dates of the pre-prostatectomy mpMRI's, all the images were re-reviewed and regraded according to the PIRADSv2 system. The radiologist is a trained genitourinary radiologist with experience in mpMRI. The radiologist identified each individual nodule that was visible on the mpMRI and applied a PIRADSv2 score, but was blinded to the location of the nodules on the prostatectomy specimen. MRI examinations were evaluated by a trained genitourinary radiologist with 6 years of experience in interpreting prostate MRI.

Each prostate was sectioned into 5 mm thick slices from base to apex, and the location of each nodule carefully annotated according to the sextant locations (Figure 1). Each prostate tumor nodule that was identified by the genitourinary pathologist was then matched to the corresponding location on the mpMRI. After all the mpMRI's for all the patients in the study were read and scored by the radiologist, each pathological nodule and nodule on MRI were reviewed as a group between the pathologists, urologists and radiologist to confirm the location or absence of MRI finding of each nodule in question. If the lesion was not visible on the mpMRI, it was marked as not visible. Visible lesions were defined as lesions with a PIRADSv2 score of 2 or more. Owing to the variations in the resolution of the MRI used for the patients, the analysis was limited to PCa nodules > 5 mm as measured on RP specimens. All patients in this cohort had their mpMRI's performed and interpreted at New York-Presbyterian Hospital with an endorectal coil, and 92% (44/48) of the patients had a 3 T MRI.

Table 1. Clinical characteristics of the prostatectomy cohort

Number of men	48	
Median age, years (IQR)	63	(57.7–69)
Median preoperative PSA, ng dl^{-1} (IQR)	4.95	(3.75–7.1)
Pathology stage		
pT2	32	66.7%
pT3	16	33.3%
Highest Gleason grade		
6	9	18.8%
7	30	62.5%
8+	9	18.8%
N+ disease (%)	3	6.3%
No. (%) of men whose father or brother had prostate cancer	9	18.4%

Pathologic evaluation

Slides of the formalin-fixed paraffin embedded (FFPE) tissue from all RP specimens were reviewed by study pathologists with genitourinary expertise (JF, KP, JMM) to confirm the pathologic characteristics (size, Gleason score, margin status, TNM stage) and the location of each tumor nodule. Frozen section slides from the institutional Biobank (EDRN protocol) were also examined. Tissue microarrays (TMAs) were constructed using 0.6 mm cores from the FFPE blocks, with each sample represented in triplicate.

Immunohistochemical analysis of ERG rearrangement and SPINK1 overexpression

Dual ERG/SPINK1 immunohistochemical (IHC) staining was applied using a commercially available antibody for ERG protein expression (ChromoMap DAB detection kit, 1:100 dilution, Ventana Medical System, Inc., Tucson, AZ, USA) and for SPINK1 (clone EPR3864 for ERG 4D4, 1:100 dilution, Abnova, Tapei City, Taiwan) on the Discovery XT biomarker platform (Ventana Medical Systems). Semi-quantitative evaluation of ERG protein nuclear expression was determined using a four-tier grading system as previously described.[22] Same approach was used to evaluate cytoplasmic SPINK1 expression. Moderate or strong staining of ⩾5% of tumor cells was considered positive for each case (Figure 2).

SPOP mutation analysis

Direct Sanger sequencing of putative *SPOP* somatic mutations was performed by standard methods following PCR amplification using specific primers as previously described.[7] Using additional tissues cores from the same archival FFPE blocks selected for TMA construction, DNA was extracted using phenol–chloroform and purified by ethanol precipitation method as previously described.[23]

Fluorescence *in situ* hybridization analysis of ERG rearrangement, PTEN deletion and CHD1 deletion

Five µm–thick tissue sections from the TMA blocks were used for *CHD1* fluorescence *in situ* hybridization (FISH) analysis, whereas full sections were utilized for *ERG* rearrangements and *PTEN* deletions. *ERG* rearrangement was identified by performing a dual-color break-apart FISH assay, using red-labeled probe (BAC clone RP11-24A11) and a green-labeled probe (BAC clone RP11-372O17), which span the centromeric and telomeric regions of *ERG*, respectively, and as previously described.[8,22] For detection of *PTEN* deletion, a gene specific probe (BAC clone CTD-2047N14) and a reference probe located at 10q25.2 (RP11-431P18) were used. For detection of *CHD1* deletion, a gene specific probe (RP11-58M12) and reporter probe that corresponded to pericentromeric sequence on chromosome 5 (RP11-429D13) were used. Deletion was defined per nucleus as fewer than two copies of the gene specific probe in the presence of two reference signals. At least 50 nuclei were evaluated per tissue core using a fluorescence microscope (Olympus BX51; Olympus Optical, Tokyo, Japan) (Figure 2).

Statistical analysis

Differences in variables with a continuous distribution across categories were assessed using the Mann–Whitney *U* test. The Fisher's exact test and the χ^2 test were used to evaluate the association between categorical variables. All tests were two-sided, with a *P*-value of < 0.05 considered to be statistically significant. All analyses were performed with STATA SE, v13.0 (StataCorp, College Station, TX, USA).

RESULTS

Clinical characteristics

Overall, 48 men underwent RP, with a median age of 63 years (IQR 58-69), and a median preoperative PSA of 4.95 ng dl^{-1} (IQR: 3.75–7.1, Table 1). The majority of the patients (67%) had pT2 disease, with 81.3% (39/48) having Gleason score 7 or above

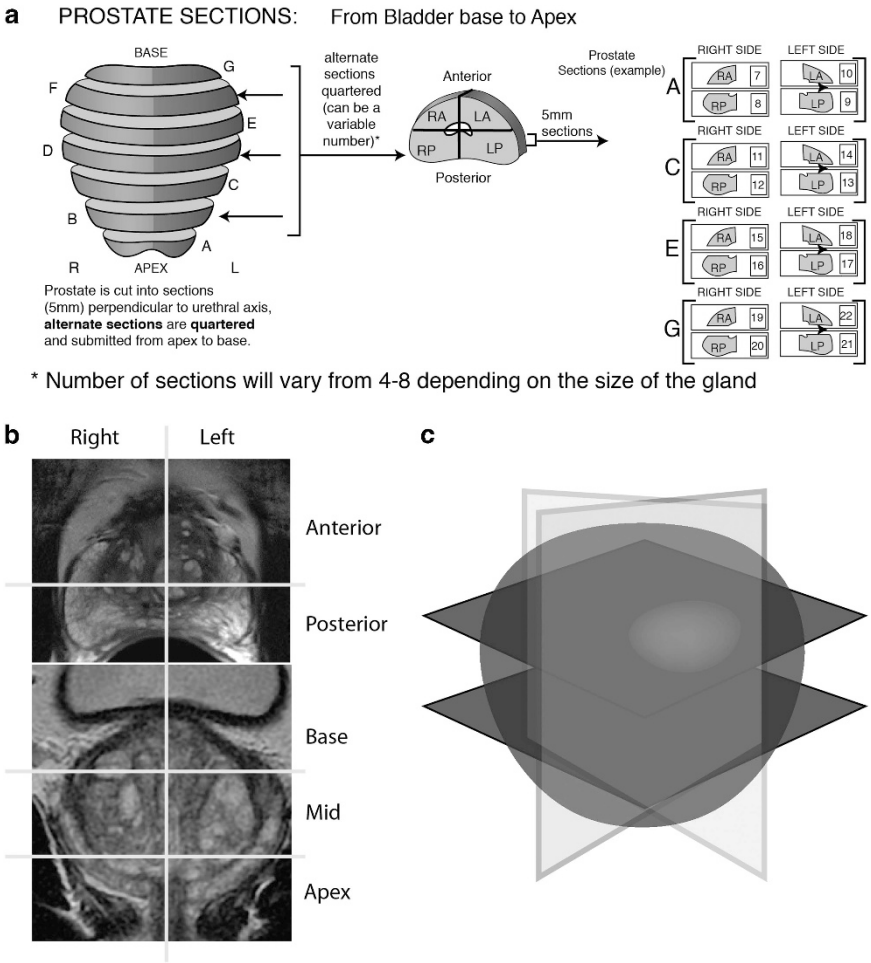

Figure 1. Schematic of anatomic correlation between pathologic processing and MRI. (**a**) Pathologic processing and biobanking protocol at Weill Cornell Medicine, consisting of alternate 0.5 cm sections, quartered along right-left, anterior-posterior axes.[31] (**b**) Representative MRI images of the prostate in axial and coronal views, with divisions into right-left, anterior-posterior and base-mid-apex. (**c**) Resulting 12 segment representation of prostate.

disease. Six percent of the men (3/48) had nodal metastasis at the time of prostatectomy.

In total, 98 PCa nodules were identified on the 48 RP specimens, with a median size of 0.7 cm (IQR: 0.3–1.3 cm, see Table 2). Of these 98 tumor nodules, 62 (63.3%) were >0.5 cm in size. Of the lesions >0.5 cm, 63% (39/62) of the nodules were Gleason 7, and 16.1% (10/62) were Gleason 8 or above. Of the 36 nodules $\leqslant 0.5$ cm, 13 (36.1%) were Gleason 7 and 23 (63.9%) were Gleason 6.

Molecular alterations

ERG expression was evaluated on 95% (60/62) of the nodules from the RP specimens, with 2 IHC failures (3%, Table 2). Of the 60 nodules that were evaluated, 35.5% (22/60) were positive for ERG overexpression. SPINK1 IHC was performed on 95% (60/62) of the nodules also, of which 10% (6/62) were positive for SPINK1 overexpression. ERG expression and SPINK1 overexpression were mutually exclusive at all times. Forty-two of the nodules (68%) were successfully evaluated for *SPOP* mutation, of which 6 (10%) were positive. FISH was performed to detect *CHD1* or *PTEN* deletions on 23% (23/62) and 43.5% (27/62) of the specimens, respectively, with positive findings for *CHD1* and *PTEN* deletions found on 17% (4/23) and 3.7% (1/27) of the specimens, respectively. These data are consistent with the reported prevalence of these alterations in other cohorts.[6–8,22,24,25]

ERG translocations were present in about 36% (17/47) of the nodules that were Gleason grade 7 or higher compared to 39% (5/13) of the nodules that were Gleason grade 6 ($P=0.34$, Table 3). *SPOP* mutations were more frequent in Gleason 7 (8%) and 8+ (30%) disease and absent in Gleason 6 disease ($P=0.04$). Although SPINK1 overexpression, *CHD1* deletions and *PTEN* deletions were only found in nodules with Gleason grade 7 or higher, there was no significant association between Gleason grade and these molecular alterations.

Association between molecular alterations and MRI findings

Overall, of the 62 nodules >0.5 cm, 40 (64.5%) were visible on mpMRI. Although a higher proportion of nodules with Gleason 7 or 8+ were visible on mpMRI compared to Gleason 6 nodules (61.5% and 90 vs 53.9%, respectively, the differences were not statistically significant ($P=0.14$). Of the visible nodules, 92% (35/38) had PIRADS scores of 4 or 5 (Table 4), with a median minimum ADC value of 662.5 (IQR: 560–797). One hundred percent of the nodules that had overexpression of SPINK1 were visible on mpMRI compared to 61% of those without SPINK1 overexpression, although the differences were not statistically significant ($P=0.06$). However, there was no significant association

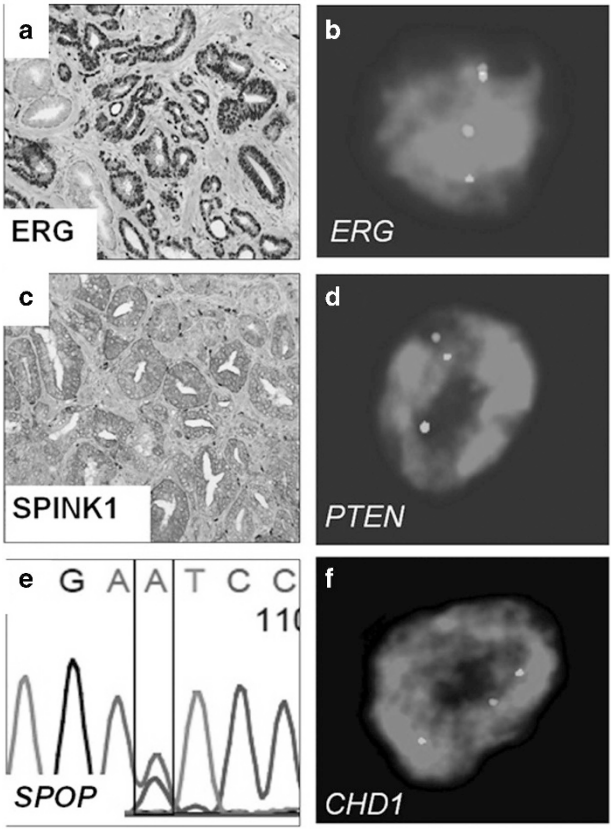

Figure 2. Recurrent molecular alterations in prostate cancer. (**a**) Representative case of ERG expression by immunohistochemistry. (**b**) Fluorescence *in situ* hybridization (FISH) break-apart assay showing *ERG* rearrangement. (**c**) FISH assay for *PTEN* showing hemizygous deletion. (**d**) Representative case of SPINK1 overexpression by immunohistochemistry. (**e**) Sanger sequencing of *SPOP* exons 6 and 7, showing mutation F133L. (**f**) FISH assay for *CHD1* showing hemizygous deletion.

between the PIRADS score or ADC values and SPINK1 overexpression ($P = 0.99$). All tumor nodules that had *CHD1* deletions were not visible on MRI, whereas 63% of those without *CHD1* deletions were visible on mpMRI ($P = 0.037$). There were no significant associations between *ERG* translocation, *SPOP* mutation, or *PTEN* deletion and characteristics on mpMRI.

On a logistic regression model predicting visibility on mpMRI, Gleason grade (odds ratio (OR) = 8.6, $P = 0.01$) and size of the nodule on the pathological specimen (OR = 5.2, $P < 0.01$) were associated with increased odds of visibility. None of the molecular or genomic alterations were associated with visibility on mpMRI on a logistic regression model. On multivariable regression model controlling for tumor size, Gleason grade, molecular changes and tumor location, there were no significant independent predictors for visibility, although there was a trend towards significance for Gleason grade (OR = 4.8, $P = 0.09$).

DISCUSSION

Advances in mpMRI have improved the detection, sampling and stratification of PCa.[17,18] Significant progress has been made in understanding the molecular basis for PCa tumorigenesis and progression, with the development of multiple biomarkers that are associated with PCa progression and biochemical recurrence-free survival. One important study found that functional and morphological features of mpMRI, such as diffusion-weighted imaging and tumor size, had a low but significant correlation with cell cycle progression scores.[26] Another more recent study found that gene expression profiles from prostate biopsy specimens were strongly associated with features on mpMRI, especially in

Table 2. Pathologic characteristics of tumor nodules in prostatectomy cohort

Number of nodules	98		Number of nodules >0.5 cm	62	
Median size of nodules, cm (IQR)	0.7	(0.3–1.3)	Median size of nodules, cm (IQR)	1	(0.8–1.6)
Gleason grade per nodule			*Gleason grade per nodule*		
6	36	36.7%	6	13	21.0%
7	52	53.1%	7	39	62.9%
8+	10	10.2%	8+	10	16.1%
ERG translocation			*ERG translocation*		
Negative	65	66.3%	Negative	38	61.3%
Positive	31	31.6%	Positive	22	35.5%
IHC failure	2	2.0%	IHC failure	2	3.2%
SPINK1 overexpression			*SPINK1 overexpression*		
Negative	83	84.7%	Negative	54	87.1%
Positive	12	13.0%	Positive	6	9.7%
IHC failure	2	2.0%	IHC failure	2	3.2%
SPOP mutation			*SPOP mutation*		
Negative	50	51.0%	Negative	36	58.1%
Positive	8	8.2%	Positive	6	9.7%
Failure/missing	40	40.8%	Failure/missing	20	32.3%
CHD1 deletion			*CHD1 deletion*		
Negative	20	20.4%	Negative	19	30.7%
Positive	4	4.1%	Positive	4	6.5%
Failure/missing	74	75.5%	Failure/missing	39	62.9%
PTEN deletion			*PTEN deletion*		
Negative	43	43.9%	Negative	26	41.9%
Positive	4	4.1%	Positive	1	1.6%
Failure/missing	51	52%	Failure/missing	35	56.5

Table 3. Pathologic characteristics of tumor nodules in prostatectomy cohort by Gleason grade nodules >0.5 cm

	Gleason grade			P-*value*
	6	*7*	*8+*	
ERG translocation				
Negative	8 (61.5%)	21 (53.9%)	9 (90%)	0.34
Positive	5 (38.5%)	16 (41%)	1 (10%)	
SPINK1 overexpression				
Negative	12 (92.3%)	33 (84.6%)	9 (90%)	0.52
Positive	1 (7.7%)	4 (10.3%)	1 (10%)	
SPOP mutation				
Negative	7 (53.9%)	25 (64.1%)	4 (40%)	0.04
Positive		3 (7.7%)	3 (30%)	
CHD1 deletion				
Negative	5 (38.5%)	13 (33.3%)	1 (10%)	0.21
Positive		3 (7.7%)	1 (10%)	
PTEN deletion				
Negative	5 (38.5%)	15 (38.5%)	6 (60%)	0.99
Positive		1 (2.6%)		

Table 4. Molecular characteristics of tumor nodules according to PIRADS score (for nodules >0.5 cm)

	Total	*ERG*			*SPINK1*			*SPOP*			*CHD1*			*PTEN*		
		Negative	*Positive*	P-*value*	*Negative*	*Overexpression*	P-*value*	*Negative*	*Mutation*	P-*value*	*Negative*	*Deletion*	P-*value*	*Negative*	*Deletion*	P-*value*
MRI findings																
Nodules not visible	22 (35.5%)	13 (34.2%)	8 (36.4%)	0.99	21 (38.9%)	0	0.06	13 (36.1%)	2 (33.3%)	0.99	7 (36.8%)	4 (100%)	0.037	11 (42.3%)	0	0.99
Nodule visible	40 (64.5%)	25 (65.8%)	14 (63.6%)		33 (61.1%)	6 (100%)		23 (63.9%)	4 (66.7%)		12 (63.2%)	0		15 (57.7%)	1 (100%)	
PIRADS score (sum)																
1 to 3	3 (7.9%)		2 (14.3%)	0.25	2 (6.5%)		0.58	3 (13.6%)		0.99	2 (16.7%)			2 (13.3%)		0.99
4	17 (44.7%)	11 (47.8%)	6 (42.9%)		13 (41.9%)	4 (66.7%)		10 (45.5%)	2 (50%)		4 (33.3%)			4 (26.7%)		
5	18 (47.4%)	12 (52.2%)	6 (42.9%)		16 (51.6%)	2 (33.3%)		9 (40.9%)	2 (50%)		6 (50%)			9 (60%)	1 (100%)	
Median ADC average	876 (690–949)															
Median ADC minimum	662.5 (560–797)															

genes associated with androgen receptor signaling.[27] However, these studies did not evaluate the most common genomic and molecular alterations in PCa, such as *SPOP* mutations and SPINK1 overexpression, that represent common and clinically important subtypes in PCa. To the best of our knowledge, this is the first study to evaluate any potential associations between the most common molecular alterations in PCa and their characteristics on mpMRI.

This study suggests a significant association between *CHD1* deletions and detection on mpMRI, and a possible association with SPINK1 overexpression. Both SPINK1 and *CHD1* are important alterations in tumorigenesis and PCa progression. SPINK1 is a protein that is overexpressed in a subset of ETS-negative PCas, and has been found to be associated with increased growth and invasion in PCa models through its interactions with the epidermal growth factor receptor (EGFR).[28,29] Recent studies have also found that SPINK1 positive tumors represent a particular aggressive subtype in PCa, and has been independently associated with biochemical recurrence-free survival and progression.[24] All SPINK1 overexpressing tumors were visible and appeared suspicious for malignancy on mpMRI, compared to a rate of 61% for those who were SPINK1 negative. This distinction may be important to help further risk-stratify PCa lesions on initial diagnosis or progression on active surveillance, as SPINK1 positive PCa represents an aggressive subtype, but may also serve as a potential marker for targeted therapy for patients with SPINK1 overexpression, towards either the SPINK1 protein or against EGFR.[28,29] Early results from clinical trials in lung cancer and PCa support the use of targeted therapy defined by distinct molecular subtypes (that is, *ERG*, *ETV1*, EGFR status), and methods to define the molecular subtypes are becoming increasingly important. If diagnostic imaging can provide further granularity in risk-prognostication by identifying molecular subclasses, then mpMRI can be an even more essential component in personalizing PCa treatment. However, further studies are needed to clarify these important molecular subtypes and their respective imaging on mpMRI.

CHD1 encodes a protein that is essential for remodeling chromatin states and transcriptional control across the genome, and is found in about 10-25% of primary and metastatic PCa lesions.[6,7] All of the lesions with *CHD1* deletions were not visible on mpMRI, compared to a rate of 37% for those without *CHD1* deletions. In light of the recent studies that supported the use of MR fusion biopsy techniques to improve the sampling and sensitivity of prostate biopsies to detect high grade PCas,[18] this group with *CHD1* deletions (and possibly tumors with SPINK1 overexpression) may represent an important subclass of aggressive PCa that may not be initially discovered, followed or evaluated by mpMRI. With increasing utilization of mpMRI and reliance on imaging modalities in the diagnosis and management of PCa,[30] it is important for future studies to substantiate these findings and identify potential aggressive subtypes that may be missed during their window of curability.

It is interesting to note that *ERG* rearrangements and *SPOP* mutations, two of the early clonal events in PCa tumorigenesis that represent distinct subclasses of primary PCa,[4,5,7] had no significant association with visibility on mpMRI or with any lesion characteristics on mpMRI. These results could suggest that the early driver lesions may not confer any visibility on mpMRI, and that secondary mutations and alterations, such as *CHD1* deletions and SPINK1 overexpression, are required to characterize the PCa with mpMRI.

Our study has several limitations that should be considered. The inter- and intratumoral heterogeneity in PCa can confound the association of specific endpoints with molecular subclasses; the use of TMAs may exacerbate this limitation. The inherent resolution limitation of mpMRI is also a limitation; it is difficult to definitively identify the presence or absence of small nodules, and so those samples were excluded *a priori*. With future

improvements in mpMRI, hopefully we can study the impact of molecular alterations in a cohort of smaller nodules. In addition, whole-mount sectioning was not used to map out the exact locations of each nodule to the mpMRI, which could represent an ascertainment bias. The overall sample size of this cohort is small; although significant differences were found in mpMRI characteristics, these findings should be best viewed as hypothesis-generating for future studies. In addition, the samples were obtained from a single institution and were reviewed retrospectively, with its inherent biases.

CONCLUSIONS

This investigation represents the first description of an association between molecular alterations and the characterization of PCa on mpMRI. These molecular alterations may help identify different subclasses in PCa by imaging modalities and potentially image-guided personalized therapies. Further investigations are required to substantiate these findings.

CONFLICT OF INTEREST

The authors declare no conflict of interest.

ACKNOWLEDGEMENTS

This study was funded by EDRN NCI U01 CA111275-09 (MAR and JMM), NCI R01 CA125612-05A1 and K08CA187417-02), the Prostate Cancer Foundation, and the Urology Care Foundation (Rising Star in Urology Research Award to CEB). CEB is a Damon Runyon Clinical Investigator supported (in part) by the Damon Runyon Cancer Research Foundation. This work was also supported in part by the Translational Research Program at WCM Pathology and Laboratory Medicine.

REFERENCES

1 Shariat S, Kattan M, Vickers A, Karakiewicz P, Scardino P. Critical review of prostate cancer predictive tools. *Future Oncol* 2009; **5**: 1555–1584.
2 Lu-Yao GL, Albertsen PC, Moore DF, Shih W, Lin Y, DiPaola RS *et al.* Outcomes of localized prostate cancer following conservative management. *JAMA* 2009; **302**: 1202–1209.
3 Resnick MJ, Penson DF. Functional outcomes after treatment for prostate cancer. *N Engl J Med* 2013; **368**: 1654.
4 Kaffenberger SD, Barbieri CE. Molecular subtyping of prostate cancer. *Curr Opin Urol* 2016; **26**: 213–218.
5 Cancer Genome Atlas Research Network. The molecular taxonomy of primary prostate cancer. *Cell* 2015; **163**: 1011–1025.
6 Grasso CS, Wu YM, Robinson DR, Cao X, Dhanasekaran SM, Khan AP *et al.* The mutational landscape of lethal castration-resistant prostate cancer. *Nature* 2012; **487**: 239–243.
7 Barbieri CE, Baca SC, Lawrence MS, Demichelis F, Blattner M, Theurillat JP *et al.* Exome sequencing identifies recurrent SPOP, FOXA1 and MED12 mutations in prostate cancer. *Nat Genet* 2012; **44**: 685–689.
8 Tomlins SA, Rhodes DR, Perner S, Dhanasekaran SM, Mehra R, Sun XW *et al.* Recurrent fusion of TMPRSS2 and ETS transcription factor genes in prostate cancer. *Science* 2005; **310**: 644–648.
9 Soller MJ, Isaksson M, Elfving P, Soller W, Lundgren R, Panagopoulos I. Confirmation of the high frequency of the TMPRSS2/ERG fusion gene in prostate cancer. *Genes Chromosomes Cancer* 2006; **45**: 717–719.
10 Yoshimoto M, Joshua AM, Chilton-Macneill S, Bayani J, Selvarajah S, Evans AJ *et al.* Three-color FISH analysis of TMPRSS2/ERG fusions in prostate cancer indicates that genomic microdeletion of chromosome 21 is associated with rearrangement. *Neoplasia* 2006; **8**: 465–469.
11 Lapointe J, Kim YH, Miller MA, Li C, Kaygusuz G, van de Rijn M *et al.* A variant TMPRSS2 isoform and ERG fusion product in prostate cancer with implications for molecular diagnosis. *Mod Pathol* 2007; **20**: 467–473.
12 Mehra R, Tomlins SA, Shen R, Nadeem O, Wang L, Wei JT *et al.* Comprehensive assessment of TMPRSS2 and ETS family gene aberrations in clinically localized prostate cancer. *Mod Pathol* 2007; **20**: 538–544.
13 Perner S, Mosquera JM, Demichelis F, Hofer MD, Paris PL, Simko J *et al.* TMPRSS2-ERG fusion prostate cancer: an early molecular event associated with invasion. *Am J Surg Pathol* 2007; **31**: 882–888.
14 Demichelis F, Setlur SR, Beroukhim R, Perner S, Korbel JO, Lafargue CJ *et al.* Distinct genomic aberrations associated with ERG rearranged prostate cancer. *Genes Chromosomes Cancer* 2009; **48**: 366–380.
15 Berg KD, Vainer B, Thomsen FB, Roder MA, Gerds TA, Toft BG *et al.* ERG protein expression in diagnostic specimens is associated with increased risk of progression during active surveillance for prostate cancer. *Eur Urol* 2014; **66**: 851–860.
16 Lindberg J, Klevebring D, Liu W, Neiman M, Xu J, Wiklund P *et al.* Exome sequencing of prostate cancer supports the hypothesis of independent tumour origins. *Eur Urol* 2013; **63**: 347–353.
17 Turkbey B, Mani H, Shah V, Rastinehad AR, Bernardo M, Pohida T *et al.* Multiparametric 3 T prostate magnetic resonance imaging to detect cancer: histopathological correlation using prostatectomy specimens processed in customized magnetic resonance imaging based molds. *J Urol* 2011; **186**: 1818–1824.
18 Siddiqui MM, Rais-Bahrami S, Turkbey B, George AK, Rothwax J, Shakir N *et al.* Comparison of MR/ultrasound fusion-guided biopsy with ultrasound-guided biopsy for the diagnosis of prostate cancer. *JAMA* 2015; **313**: 390–397.
19 Prensner JR, Chinnaiyan AM, Srivastava S. Systematic, evidence-based discovery of biomarkers at the NCI. *Clin Exp Metastasis* 2012; **29**: 645–652.
20 Srivastava S, Rossi SC. Early detection research program at the NCI. *Int J Cancer* 1996; **69**: 35–37.
21 American College of Radiology. MR prostate imaging reporting and data system version 2.0. Available at http://www.acr.org/Quality-Safety/Resources/PIRADS/. Accessed April 2017.
22 Park K, Tomlins SA, Mudaliar KM, Chiu YL, Esgueva R, Mehra R *et al.* Antibody-based detection of ERG rearrangement-positive prostate cancer. *Neoplasia* 2010; **12**: 590–598.
23 Berger MF, Lawrence MS, Demichelis F, Drier Y, Cibulskis K, Sivachenko AY *et al.* The genomic complexity of primary human prostate cancer. *Nature* 2011; **470**: 214–220.
24 Terry S, Nicolaiew N, Basset V, Semprez F, Soyeux P, Maille P *et al.* Clinical value of ERG, TFF3, and SPINK1 for molecular subtyping of prostate cancer. *Cancer* 2015; **121**: 1422–1430.
25 Yoshimoto M, Joshua AM, Cunha IW, Coudry RA, Fonseca FP, Ludkovski O *et al.* Absence of TMPRSS2:ERG fusions and PTEN losses in prostate cancer is associated with a favorable outcome. *Mod Pathol* 2008; **21**: 1451–1460.
26 Renard-Penna R, Cancel-Tassin G, Comperat E, Varinot J, Léon P, Roupret M *et al.* Multiparametric magnetic resonance imaging predicts postoperative pathology but misses aggressive prostate cancers as assessed by cell cycle progression score. *J Urol* 2015; **194**: 1617–1623.
27 Stoyanova R, Pollack A, Takhar M, Lynne C, Parra N, Lam LL *et al.* Association of multiparametric MRI quantitative imaging features with prostate cancer gene expression in MRI-targeted prostate biopsies. *Oncotarget* 2016; **7**: 53362–53376.
28 Tomlins SA, Rhodes DR, Yu J, Varambally S, Mehra R, Perner S *et al.* The role of SPINK1 in ETS rearrangement-negative prostate cancers. *Cancer Cell* 2008; **13**: 519–528.
29 Ateeq B, Tomlins SA, Laxman B, Asangani IA, Cao Q, Cao X *et al.* Therapeutic targeting of SPINK1-positive prostate cancer. *Sci Transl Med* 2011; **3**: 72ra17.
30 Porten SP, Smith A, Odisho AY, Litwin MS, Saigal CS, Carroll PR *et al.* Updated trends in imaging use in men diagnosed with prostate cancer. *Prostate Cancer Prostatic Dis* 2014; **17**: 246–251.
31 Esgueva R, Park K, Kim R, Kitabayashi N, Barbieri CE, Dorsey PJ *et al.* Next-generation prostate cancer biobanking: toward a processing protocol amenable for the International Cancer Genome Consortium. *Diagn Mol Pathol* 2012; **21**: 61–68.